Bending elasticity and thermal fluctuations of lipid membranes. Theoretical and experimental requirements

J.F. Faucon, M. D. Mitov, P. Méléard, I. Bivas, P. Bothorel

Bending elasticity and thermal fluctuations of lipid membranes.
Theoretical and experimental requirements

J. F. Faucon ([1]), M. D. Mitov ([2]), P. Méléard ([1]), I. Bivas ([2]) and P. Bothorel ([1])

([1]) Centre de Recherche Paul Pascal, C.N.R.S., Domaine Universitaire, 33405 Talence, France
([2]) Department of Liquid Crystals, Institute of Solid State Physics, Bulgarian Academy of Sciences, Sofia 1784, Bulgaria

Résumé. — Les fluctuations thermiques de vésicules lipidiques géantes ont été étudiées d'un point de vue théorique et expérimental. Au niveau théorique, le modèle développé prend explicitement en compte la conservation du volume de la vésicule et de la surface de la membrane. Il en résulte que l'amplitude des fluctuations thermiques dépend non seulement de l'élasticité de courbure de la bicouche, mais aussi de la tension de membrane et/ou de la différence de pression hydrostatique entre l'intérieur et l'extérieur de la vésicule. Au niveau expérimental, la détermination du module de courbure k_c nécessite d'abord l'analyse d'un grand nombre (plusieurs centaines) de contours afin d'obtenir une bonne statistique. En second lieu, la contribution de l'erreur expérimentale sur les coordonnées du contour, qui se traduit par un bruit blanc sur les amplitudes de Fourier, doit être éliminée, et ceci peut être réalisé grâce à l'utilisation de la fonction d'autocorrélation angulaire des fluctuations. Enfin, les amplitudes des harmoniques ayant des temps de corrélation courts doivent être corrigées de l'effet du temps d'intégration (40 ms) de la caméra vidéo, qui, dans le cas contraire, conduit à une surestimation de k_c. Toutes ces exigences théoriques et expérimentales ont été prises en compte dans l'analyse des fluctuations thermiques de 42 vésicules géantes de phosphatidylcholine du jaune d'œuf. Il peut être rendu compte du comportement de cette population de vésicules avec un module de courbure k_c égal à $0.4 - 0.5 \times 10^{-19}$ J, et des tensions de membrane extrêmement faibles, de moins de 15×10^{-5} mN/m.

Abstract. — Thermal fluctuations of giant lipid vesicles have been investigated both theoretically and experimentally. At the theoretical level, the model developed here takes explicitly into account the conservation of vesicle volume and membrane area. Under these conditions, the amplitude of thermal fluctuations depends critically not only on the bending elasticity of the bilayer, but also on the membrane tension and/or hydrostatic pressure difference between the interior and exterior of the vesicle. At the experimental level, the determination of the bending modulus k_c first requires the analysis of a large number (several hundred) of vesicle contours to obtain a significant statistics. Secondly, the contribution of the experimental error on the contour coordinates, which results in a white noise on the Fourier amplitudes, must be eliminated, and this can be done by using the angular autocorrelation function of the fluctuations. Finally, the amplitudes of harmonics having short correlation times must be corrected from the effect of the integration time (40 ms) of the video camera, which otherwise leads to an overestimation of k_c. All these theoretical and experimental requirements have been considered in the analysis of the thermal fluctuations of 42 giant vesicles composed of egg phosphatidylcholine. The behaviour

of this population of vesicles can be accounted for with a bending modulus k_c equal to $0.4 - 0.5 \times 10^{-19}$ J, and extremely low membrane tensions, ranging below 15×10^{-5} mN/m.

1. Introduction.

Biological membranes are an essential constituent of every living cell. Their mechanical properties are closely related to the problem of cell stability and resistance to external influences, and hence have become the subject of increased attention. Considering the membrane as an infinitely thin layer of liquid crystal and applying the ideas of liquid crystal physics, Helfrich [1] has demonstrated that the mechanical state of a membrane element can be completely characterized specifying its area and principal curvatures. The stretching elastic energy per unit area, F_s, is given by the expression [1] :

$$F_s = \frac{k_s}{2} \left(\frac{\Delta S}{S_0} \right)^2 \qquad (\Delta S = S - S_0) \qquad (1)$$

$$\sigma = S_0 \frac{\partial F_s}{\partial S} = k_s \left(\frac{\Delta S}{S_0} \right) \qquad (2)$$

where σ is the bilayer tension, S_0 is the equilibrium area of the membrane element (e.g. the area at zero membrane tension), S is the deformed area of the same element, and k_s is the stretching elastic constant. The mechanical experiments of Kwok and Evans [2, 3] yield $k_s = (140 \pm 16)$ mJ/m^2 for egg lecithin bilayers.

When a small piece of membrane is bent, the bending elastic energy per unit area, F_c, is given, according to Helfrich [1], by the expression :

$$F_c = \frac{k_c}{2} (c_1 + c_2 - c_0)^2 + \bar{k}_c \, c_1 \, c_2 \qquad (3)$$

where c_1 and c_2 are the principal curvatures of the membrane, c_0 is the spontaneous curvature ($c_0 \neq 0$ if the two monolayers have different composition or they face different environments), k_c and $\bar{k}_c$ are the elastic constants for cylindrical bending and saddle bending, respectively.

The first attempt to measure the curvature elastic modulus, k_c, was made by Servuss et al. [4]. Analysing the thermal shape fluctuations of long tubular vesicles they obtained $k_c = (2.3 \pm 0.3) \times 10^{-19}$ J, for egg lecithin membranes. Later on, Sakurai and Kawamura [5] evaluated $k_c = 0.4 \times 10^{-19}$ J by bending myelin figures in a magnetic field. Measuring the time correlation function of the shape fluctuations of long cylindrical tubes [6], as well as giant spherical vesicles [7], Schneider et al. found $k_c = (1 - 2) \times 10^{-19}$ J. Using Fourier analysis of thermally excited surface undulations of vesicles, Engelhardt et al. [8] obtained $k_c = 0.4 \times 10^{-19}$ J. Recently, Duwe et al. [9] reported $k_c = 1.1 \times 10^{-19}$ J. Introducing the angular correlation function of thermal shape fluctuations, Bivas et al. [15] measured $k_c = (1.28 \pm 0.25) \times 10^{-19}$ J.

In contrast to the measurements of stretching elastic constant, k_s, where a single value has been reported, there is a great variety between the values measured by various authors $k_c = (0.4 - 2.3) \times 10^{-19}$ J. Different explanations for these variations have been put forward by the authors, but rarely acceptable arguments have been given, except in [10]. Obviously, there is an appealing necessity for more precise treatment of this important question. The aim of this article is to analyze in detail potential sources of theoretical, as well as experimental errors and to explore different possibilities for overcoming them.

2. Theory.

To a very good approximation, the vesicle membrane can be considered as a two-dimensional (geometrical) surface. Using spherical polar coordinates (r, θ, φ), with origin O in the center of the vesicle, we can describe a slightly deformed spherical vesicle by writing :

$$r(\theta, \varphi, t) = R[1 + u(\theta, \varphi, t)] \tag{4}$$

where R is the radius of a sphere enclosing the same volume as that of the vesicle, and $u(\theta, \varphi, t)$ is a function describing the relative displacements (the fluctuations) of the vesicle wall from the ideal spherical shape, θ and φ being the polar angles. It is assumed in what follows that the amplitudes of the fluctuations are very small compared to the vesicle dimensions, $|u(\theta, \varphi, t)| \ll 1$.

As far as we have chosen the origin of the coordinate system in the center of the vesicle we have by definition :

$$\iint u(\theta, \varphi, t) Y_1^m(\theta, \varphi) \sin \theta \, d\theta \, d\varphi = 0 , \qquad m = -1, 0, 1 \tag{5}$$

where $Y_1^m(\theta, \varphi)$ are the spherical harmonics defined below.

The volume of the vesicle, $\mathcal{V}\{u\}$, is given by the expression :

$$\mathcal{V}\{u\} = \iint V(u) \, d\theta \, d\varphi \qquad \mathcal{V}_0 = \frac{4\pi}{3} R^3 \tag{6}$$

$$V(u) = R^3 \left(\frac{1}{3} + u + u^2 \right) \sin \theta .$$

Here, $\mathcal{V}_0$ denotes the volume of a sphere of radius R, and we have kept only the terms of first and second order with respect to u.

Similarly, the deformed area of the vesicle, $\mathcal{S}\{u\}$, is given by the expression :

$$\mathcal{S}\{u\} = \iint S(u, u_\theta, u_\varphi) \, d\theta \, d\varphi , \qquad \mathcal{S}_0 = 4\pi R^2 (1 + s) \tag{7}$$

$$S(u, u_\theta, u_\varphi) = R^2 \left[1 + 2u + u^2 + \frac{1}{2} \left(u_\theta^2 + \frac{u_\varphi^2}{\sin^2 \theta} \right) \right] \sin \theta$$

where u_θ and u_φ stand for the partial derivatives of u with respect to parameters θ and φ, respectively, $\mathcal{S}_0$ is the total vesicle area at zero membrane tension and s is the area in excess over that of a sphere of equivalent volume. Here again we have kept only the terms of first and second order with respect to u and its derivatives.

The lipid bilayers behave like two-dimensional liquids, therefore every local variation of the membrane tension is rapidly relaxed *via* local flows of the lipid material resulting in $\sigma = \text{const.}$ all over the membrane. As a consequence, the stretching elastic energy of the whole vesicle, $\mathcal{F}_s\{u\}$, as well as the membrane tension, σ, may be written in a global form :

$$\mathcal{F}_s\{u\} = \frac{k_s}{2 \mathcal{S}_0} \left[\iint S(u, u_\theta, u_\varphi) \, d\theta \, d\varphi - \mathcal{S}_0 \right]^2 \tag{8}$$

$$\sigma = \frac{k_s}{\mathcal{S}_0} \left[\iint S(u, u_\theta, u_\varphi) \, d\theta \, d\varphi - \mathcal{S}_0 \right] \tag{9}$$

The bending elastic energy of the vesicle, $\mathcal{F}_c\{u\}$, is given by the expression :

$$\mathcal{F}_c\{u\} = \iint F_c(u, u_\theta, u_\varphi, u_{\theta\theta}, u_{\varphi\varphi}) \, \mathrm{d}\theta \, \mathrm{d}\varphi \tag{10}$$

$$F_c = \frac{k_c}{2}\left[4 - 4\,\nabla^2 u + 4\,u\,\nabla^2 u + (\nabla^2 u)^2 + 2(\nabla u)^2\right]\sin\theta$$

$$(\nabla u)^2 = \left(u_\theta^2 + \frac{u_\varphi^2}{\sin^2\theta}\right) \qquad \nabla^2 u = \left(u_{\theta\theta} + \frac{\cos\theta}{\sin\theta}u_\theta + \frac{u_{\varphi\varphi}}{\sin^2\theta}\right)$$

where $u_{\theta\theta}$ and $u_{\varphi\varphi}$ stand for the second partial derivatives of the function u with respect to parameters θ or φ, respectively. When integrated over the closed vesicle surface, the Gaussian curvature term (the second term in the equation (3)) gives a constant value, $4\pi\bar{k}_c$, independent of the vesicle shape [11, 12], and it can therefore be omitted. We have kept again only the terms of first and second order with respect to u and its derivatives.

Usually, vesicles are poorly permeable to water and salts, and to a very good approximation water is an uncompressible fluid. So, we shall consider that the vesicle volume does not change during the fluctuations, and therefore the following condition always holds :

$$\mathcal{V}\{u\} = \mathcal{V}_0 \qquad \text{or} \qquad \iint V(u)\,\mathrm{d}\theta\,\mathrm{d}\varphi = \frac{4\pi}{3}R^3 \tag{11}$$

The fluctuations of the vesicle membrane are time dependent thermal agitations around the equilibrium vesicle form. Thus, we can consider the vesicle shape at a given moment, $u(\theta, \varphi, t)$, as composed of two contributions : a static part, $u_0(\theta, \varphi)$, that is the average (equilibrium) vesicle shape and a dynamic part or perturbation, $\delta u(\theta, \varphi, t)$, that gives the deviation from this equilibrium and describes the fluctuations of the vesicle :

$$u(\theta, \varphi, t) = u_0(\theta, \varphi) + \delta u(\theta, \varphi, t) \tag{12}$$

$$\langle u(\theta, \varphi, t)\rangle = u_0(\theta, \varphi) \Rightarrow \langle \delta u(\theta, \varphi, t)\rangle = 0 .$$

The angle brackets in the above equation denote an ensemble or time average. It is natural to suppose that the ergodic hypothesis holds when there are no temporal drifts or changes in the environmental conditions during the experiment.

To find the equilibrium vesicle shape, we have to minimize the total energy, keeping the volume constant. This is a variational problem *with* a constraint. The usual method to solve it is to replace the original functional and the associated constraint with a new functional, $\mathcal{F}\{u\}$, that is a linear combination of them and to treat the last like a functional without constraint, so we write :

$$\mathcal{F}\{u\} = \mathcal{F}_c\{u\} + \mathcal{F}_s\{u\} - \Delta p\,\mathcal{V}\{u\} . \tag{13}$$

Here, Δp is Lagrange multiplier associated with the constraint of constant vesicle volume (physically, Δp is the hydrostatic pressure difference acting across the vesicle membrane). If the function u_0 minimizes the functional (13) then its first variation, $\delta\mathcal{F}\{u_0, \delta u\}$, is zero for all small perturbations, δu, around this equilibrium shape, u_0 :

$$\delta\mathcal{F}\{u_0, \delta u\} = \delta\mathcal{F}_c\{u_0, \delta u\} + \sigma\,\delta\mathcal{S}\{u_0, \delta u\} - \Delta p\,\delta\mathcal{V}\{u_0, \delta u\} = 0 . \tag{14}$$

It is well known that if a function u_0 satisfies a condition like (14), this function is a solution of the Euler-Lagrange equation associated with this variational problem. The explicit form of the Euler-Lagrange equation in our case is :

$$\nabla^2(\nabla^2 u_0) + (2 - \bar{\sigma}) \nabla^2 u_0 + 2(\bar{\sigma} - \bar{p}) u_0 = \bar{p} - 2 \bar{\sigma} \tag{15}$$

$$\bar{p} = \frac{\Delta p R^3}{k_c} + 2 c_0 R \qquad \bar{\sigma} = \frac{\sigma R^2}{k_c} + 2 c_0 R + \frac{c_0^2 R^2}{2} .$$

Here, $\bar{p}$ and $\bar{\sigma}$ are the effective dimensionless pressure and tension, respectively, and c_0 is the spontaneous membrane curvature. Equation (15) is linear because of the quadratic approximation used throughout in this work. If the same problem is treated without approximations a forth order nonlinear partial differential equation, similar to those of Deuling and Helfrich [11, 12] and of Jenkins [17], would be obtained instead. It is inhomogeneous because the vesicle radius is given by $(1 + u_0)$, and not by u_0 itself. In the spherical case, $u_0 = $ const., equation (15) transforms into the well known Laplace law, $\bar{p} = 2 \bar{\sigma}/(1 + u_0)$, thus it can be considered as a natural generalisation of Laplace law for the case of an arbitrarily deformed closed membrane possessing curvature and stretching elasticity.

All the functions that are extremals of the functional (13) are solutions of the Euler-Lagrange equation (15). In the case that u_0 is a function that *minimizes* $\mathcal{F} \{u_0\}$ we must have :

$$\delta^2 \mathcal{F} \{u_0, \delta u\} = \delta^2 \mathcal{F}_c \{u_0, \delta u\} + \sigma \delta^2 S \{u_0, \delta u\} - \Delta p \, \delta^2 \mho \{u_0, \delta u\} +$$

$$+ \frac{k_s}{S_0} \delta S \{u_0, \delta u\} \, \delta S \{u_0, \delta u\} \geqslant 0 . \tag{16}$$

The last term in the above equation represents the contributions originating from the fluctuations of the total vesicle area and conjugated to them fluctuations of the membrane tension. Generally, the second variation of a functional like (16), the last term excluded, is a quadratic form of the perturbations δu and its derivatives $(\delta u_\theta, \delta u_\varphi, \delta u_{\theta\theta}, \delta u_{\varphi\varphi})$ with coefficients depending on the function u_0. But it can be always transformed, *via* integrations by parts, into a more convenient form :

$$\iint \delta u [\mathcal{L} \{u_0\} \, \delta u] \, d\theta \, d\varphi \tag{17}$$

where $\mathcal{L} \{u_0\}$ is a linear differential operator acting on the perturbations δu. It is convenient to expand the perturbations, δu, in a series of the eigenfunctions of the operator $\mathcal{L} \{u_0\}$. In the case of our quadratic approximation the dependence of $\mathcal{L} \{u_0\}$ on u_0 disappears and the eigenfunction equation obtains the very simple form :

$$\nabla^2(\nabla^2 \delta u) + (2 - \bar{\sigma}) \nabla^2 \delta u + 2(\bar{\sigma} - \bar{p}) \delta u = \lambda \, \delta u \tag{18}$$

The eigenfunctions are the well known spherical harmonics, $Y_n^m(\theta, \varphi)$, defined as (see [14]) :

$$Y_n^m(\theta, \varphi) = (-1)^m \sqrt{\frac{2 n + 1}{4 \pi} \frac{(n - m)!}{(n + m)!}} P_n^m(\cos \theta) e^{im\varphi} \tag{19}$$

and the corresponding eigenvalues are :

$$\lambda_n(\bar{\sigma}, \bar{p}) = n^2(n + 1)^2 - (2 - \bar{\sigma}) n(n + 1) + 2(\bar{\sigma} - \bar{p}) . \tag{20}$$

We represent δu in a series of $Y_n^m(\theta, \varphi)$. But, when writing such a series one has to take into account that there is a « high frequency » cut-off due to the discrete structure of the membrane, so we include only the terms up to $n_{\max} \approx \sqrt{N}$ (N is the number of lipid molecules constituting the vesicle). Here $n_{\max}$ is so selected that the number of independent amplitudes is equal to the number of lipid molecules. The exact value of $n_{\max}$ is not of great importance because we shall see further on that the physical quantities are only logarithmically dependent on it. Using the eigenfunctions of equation (18) we can write :

$$\delta u(\theta, \varphi, t) = \sum_{n=0}^{n_{\max}} \sum_{m=-n}^{m=+n} U_n^m(t) Y_n^m(\theta, \varphi) \tag{21}$$

where $U_n^m(t)$ are the time dependent coefficients in the expansion. Using equations (21, 12, 5) we obtain :

$$U_1^m(t) = - \iint u_0(\theta, \varphi) Y_1^m(\theta, \varphi) \sin \theta \, d\theta \, d\varphi = 0 . \tag{22}$$

This equation clearly shows that the amplitudes $U_1^m(t)$ are not time dependent. Therefore, they do not describe fluctuations. Moreover, using the second equation in (12), $\langle \delta u \rangle = 0$, and the orthogonality of the spherical harmonics, one can conclude that $\langle U_n^m(t) \rangle = 0$, and so do $U_1^m(t) = 0$. Now we can readily calculate the second variation. Substituting (21) into (17), and thereafter into (16), we obtain :

$$\frac{1}{2} \delta^2 \mathcal{F} = \frac{4 k_s R^2 + k_c \lambda_0(\bar{\sigma}, \bar{p})}{2} |U_0^0(t)|^2 + \frac{k_c}{2} \sum_{n=2}^{n_{\max}} \lambda_n(\bar{\sigma}, \bar{p}) \sum_{m=-n}^{m=+n} |U_n^m(t)|^2 . \tag{23}$$

Expression (23) gives the increase of the vesicle energy due to the thermal fluctuations as a sum of the squared amplitudes of the different modes of agitation. The k_s-term in it is the only second order contribution coming from the last term in equation (16), all the others being of higher orders, and thus neglected. If the coefficients $\lambda_n(\bar{\sigma}, \bar{p})$ are positive, one can obtain the mean-squared value of each amplitude, $\langle |U_n^m(t)|^2 \rangle$, applying the equipartition theorem to each mode of agitation :

$$\langle |U_0^0(t)|^2 \rangle = \frac{kT}{4 k_s R^2 + k_c \lambda_0(\bar{\sigma}, \bar{p})}$$

$$\langle |U_n^m(t)|^2 \rangle = \frac{kT}{k_c} \frac{1}{\lambda_n(\bar{\sigma}, \bar{p})} \qquad n \geq 2 . \tag{24}$$

If we take $kT = 4 \times 10^{-21}$ J, $k_s = 100$ mJ/m^2, $R = 10^{-5}$ m (10 μm), we calculate $\langle |U_0^0(t)|^2 \rangle = 10^{-10}$. This means that the fluctuations of the mean vesicle radius are very small.

Now we proceed further and look for a solution of the Euler-Lagrange equation (15) in series of spherical harmonics :

$$u_0(\theta, \varphi) = \sum_{n=0}^{n_{\max}} \sum_{m=-n}^{m=+n} A_n^m Y_n^m(\theta, \varphi) \tag{25}$$

where A_n^m are constants that have to be determined. Substituting the expansion (25) into the differential equation (15), one obtains a system of ordinary equations equivalent to it :

$$-\frac{A_0^0}{\sqrt{4\pi}} = \frac{\bar{p} - 2\bar{\sigma}}{2\bar{p} - 2\bar{\sigma}}, \qquad \lambda_n(\bar{\sigma}, \bar{p}) A_n^m = 0 . \tag{26}$$

It is easily seen that for each $n \neq 0$, there are two possibilities : either $\lambda_n(\bar{\sigma}, \bar{p}) = 0$ or $A_n^m = 0$. As far as $\lambda_n(\bar{\sigma}, \bar{p})$ depends on the index n, if for a given value n we have $\lambda_n(\bar{\sigma}, \bar{p}) = 0$, then for all the others we would have $\lambda_n(\bar{\sigma}, \bar{p}) \neq 0$, and therefore $A_n^m = 0$. Using equations (25, 22), we obtain $A_1^m + U_1^m(t) = 0$ and as far as $U_1^m(t) = 0$, we have $A_1^m = 0$ as well. Thus, the series expansion (25) is reduced either to a single term (A_0^0 only), and the equilibrium shape of the vesicle is spherical, or to a sum of a few terms (A_0^0 and the different amplitudes A_n^m of any given order n). However, starting from a spherical vesicle and increasing the excess area (7), the $n = 2$ eigenvalue $\lambda_2(\bar{\sigma}, \bar{p})$ will first vanish for given values of $\bar{\sigma}$ and $\bar{p}$. A sphere to ellipsoid transition should then occur leading to a non-zero average value for the $n = 2$ mode ($A_2^m \neq 0$).

The equation of Euler-Lagrange (15) as well as its equivalent form (26) contains two parameters, $\bar{\sigma}$ and $\bar{p}$. Therefore, we need two supplementary conditions to determine them. These are equations (9) and (11). Using the series expansions (21, 25), these supplementary conditions satisfied by the functions $u_0(\theta, \varphi)$ and $\delta u(\theta, \varphi, t)$ are transformed into relations between the amplitudes A_n^m and $U_n^m(t)$:

$$\frac{A_0^0 + U_0^0(t)}{\sqrt{4\pi}} + \frac{1}{4\pi} \sum_{n=0}^{n_{\max}} \sum_{m=-n}^{m=+n} \left| A_n^m + U_n^m(t) \right|^2 = 0 \tag{27}$$

$$\frac{\bar{\sigma}(t) k_c}{k_s R^2} + s = 2 \frac{A_0^0 + U_0^0(t)}{\sqrt{4\pi}} + \sum_{n=0}^{n_{\max}} \frac{n^2 + n + 2}{8\pi} \sum_{m=-n}^{m=+n} \left| A_n^m + U_n^m(t) \right|^2 \tag{28}$$

where s is the excess area defined in (7). The above two equations must hold for each moment of time, and therefore, the membrane tension, $\bar{\sigma}(t)$, is a function of time determined by equation (28). These fluctuations of the membrane tension give rise to the last term in the second variation (16) as already pointed. We see that as far as equation (27) holds, $U_0^0(t)$ is of second order instead of first (as expected a priori), and therefore, it may be always dropped when squared. Because $U_1^m(t) = 0$ as already mentioned, the summation on n in equations (27, 28) can start from $n = 2$. Furthermore, since the equilibrium shape of the vesicle is time independent we can take a time average of both equations :

$$\frac{A_0^0}{\sqrt{4\pi}} = \frac{1}{4\pi} \sum_{n=2}^{n_{\max}} \sum_{m=-n}^{m=+n} \left[\left| A_n^m \right|^2 + \left\langle \left| U_n^m(t) \right|^2 \right\rangle \right] = 0 \tag{29}$$

$$\frac{\bar{\sigma} k_c}{k_s R^2} + s = 2 \frac{A_0^0}{\sqrt{4\pi}} + \sum_{n=2}^{n_{\max}} \frac{n^2 + n + 2}{8\pi} \sum_{m=-n}^{m=+n} \left[\left| A_n^m \right|^2 + \left\langle \left| U_n^m(t) \right|^2 \right\rangle \right] . \tag{30}$$

We have to stress now that it is the mean value of the membrane tension, $\bar{\sigma} = \langle \bar{\sigma}(t) \rangle$, that enters the above equation. One can readily see that the equilibrium shape of the vesicle (given by the ampliudes, A_n^m) is influenced by the presence of the fluctuations, $\left\langle \left| U_n^m(t) \right|^2 \right\rangle$, whose mean squared values are determined by the equipartition theorem. Substituting (24) into (29,

30) one can finally obtain the relations that determine the equilibrium shape of the vesicle. In the case of a single term we have :

$$\frac{\bar{p} - 2\,\bar{\sigma}}{2\,\bar{p} - 2\,\bar{\sigma}} = \frac{kT}{4\,k_s\,R^2 + k_c\,\lambda_0(\bar{\sigma}, \bar{p})} + \frac{kT}{4\,\pi k_c} \sum_{n=2}^{n_{\max}} \frac{(2\,n+1)}{\lambda_n(\bar{\sigma}, \bar{p})}$$

$$\frac{\bar{\sigma}\,k_c}{k_s\,R^2} = \left(\frac{kT}{8\,\pi k_c} \sum_{n=2}^{n_{\max}} \frac{(n-1)(n+2)(2\,n+1)}{\lambda_n(\bar{\sigma}, \bar{p})} - s \right) \tag{31}$$

$$-\frac{A_0^0}{\sqrt{4\,\pi}} = \frac{\bar{p}(s) - 2\,\bar{\sigma}(s)}{2\,\bar{p}(s) - 2\,\bar{\sigma}(s)}$$

$$\lambda_n(\bar{\sigma}, \bar{p}) \neq 0 \Rightarrow A_n^m = 0 \,.$$

Equation (28) contains the excess area, s, as a parameter and the average shape of the vesicle depends critically on its value. The first two equations in (31) impose an implicit dependence of the mean membrane tension, $\bar{\sigma}(s)$, and the hydrostatic pressure, $\bar{p}(s)$, on the excess area, s, and therefore $\lambda_n(\bar{\sigma}(s), \bar{p}(s))$ is determined via (20) as well. The third of them gives the value of A_0^0. Here, $A_n^m = 0$ (for $n \geq 1$) and the average vesicle shape is spherical. At a given critical value of the excess area, s_{cr}, (determined from the condition : $\lambda_2(\bar{\sigma}(s_{cr}), \bar{p}(s_{cr})) = 0$) the amplitudes A_2^m are not zero anymore, and thereafter, for any value satisfying the relation $s \geq s_{cr}$ we have :

$$\lambda_2(\bar{\sigma}, \bar{p}) = 0 \quad \Rightarrow \quad \bar{p} = 12 + 4\,\bar{\sigma}$$

$$\frac{\bar{\sigma}\,k_c}{k_s\,R^2} = \left(\frac{12 + 2\,\bar{\sigma}}{12 + 3\,\bar{\sigma}} + \frac{kT}{8\,\pi k_c} \sum_{n=3}^{n_{\max}} \frac{(n^2 + n - 6)(2\,n+1)}{\lambda_n(\bar{\sigma}, \bar{p})} - s \right) - \frac{A_0^0}{\sqrt{4\,\pi}} = \frac{6 + \bar{\sigma}}{12 + 3\,\bar{\sigma}} \tag{32}$$

$$\frac{1}{4\,\pi} \sum_{m=-2}^{m=+2} |A_2^m|^2 = \frac{6 + \bar{\sigma}}{12 + 3\,\bar{\sigma}} - \frac{kT}{4\,\pi k_c} \sum_{n=3}^{n_{\max}} \frac{(2\,n+1)}{\lambda_n(\bar{\sigma}, \bar{p})} \,.$$

Here again the first two equations of (32) impose an implicit dependence of the membrane tension, $\bar{\sigma}(s)$, and the hydrostatic pressure, $\bar{p}(s)$, on the excess area, s, and the last two of them determine the vesicle shape via the amplitudes A_0^0 and A_2^m. In the case $s \geq s_{cr}$ the vesicle fluctuates around an elliptical equilibrium shape $\left(\sum_{m=-2}^{m=+2} |A_2^m|^2 \neq 0 \right)$. We point out that it is $\sum_{m=-2}^{m=+2} |A_2^m|^2$ that is determined by the last of the above equations, the sign and the relative proportion of different m-modes being undetermined. This is a consequence of the quadratic approximation used. Higher order terms must be included to discriminate between prolate and oblate ellipsoids (see [10] for more detailed discussion) and to fix the relative proportion of different m-modes (to be published).

As far as the vesicle tension, $\bar{\sigma}(s)$, and hydrostatic pressure, $\bar{p}(s)$, depend on the excess area, s, it follows from (24) that the mean squared value of the fluctuations, $\langle |U_n^m(t)|^2 \rangle$, will depend on it as well :

$$\langle |U_n^m(t)|^2 \rangle = \frac{kT}{k_c} \frac{1}{(n-1)(n+2)[\bar{\sigma} + n(n+1)] + 2(2\,\bar{\sigma} - \bar{p})} \,. \tag{33}$$

For a spherical vesicle, as long as the fluctuations are not too big (e.g. when the quadratic approximation is valid) the last term in the denominator is very small ($\bar{p} \approx 2\,\bar{\sigma}$), and

therefore, it can be omitted. Then equation (33) is transformed into the expression (34) previously obtained by Milner and Safran [10] :

$$\langle |U_n^m(t)|^2 \rangle = \frac{kT}{k_c} \frac{1}{(n-1)(n+2)[\bar{\sigma} + n(n+1)]} . \tag{34}$$

The neglected term in (33) becomes of importance in the case of an ellipsoidal vesicle (e.g. relatively bigger excess area). In this case $\bar{\sigma} + 6 = 0$, according to Milner and Safran [10], and therefore the membrane tension does not vary when the excess area, s, is changed. The amplitudes of the elliptical modes ($n = 2$, $|m| \leqslant 2$) adjust themselves to fit the available excess area. In our model it is $\lambda_2(\bar{\sigma}, \bar{p})$ that vanishes, the membrane tension, $\bar{\sigma}(s)$, and the hydrostatic pressure, $\bar{p}(s)$ are functions of the excess area, s. We have $\bar{\sigma} \approx -6$ ($\bar{p} \approx -12$), both becoming more and more negative when the excess area is increased. This result is in agreement with the conclusions made by Deuling and Helfrich [11, 12] as well as those of Jenkins [17], both obtained on the basis of numerical solution of the exact nonlinear equivalent of our Euler-Lagrange equation (15). The static amplitudes of the second harmonics, $\sum\limits_{m=-2}^{m=+2} |A_2^m|^2$, adjust themselves, according to (32), to fit the excess area as well.

We need to find a practical method for determining the mean membrane tension, $\bar{\sigma}$. According to equation (34) the product :

$$\langle |U_n^m(t)|^2 \rangle (n-1)(n+2)[\bar{\sigma} + n(n+1)] = \frac{kT}{k_c} . \tag{35}$$

is independent of n as seen from the right-hand sides of the above equations. This result can be effectively used to determine $\bar{\sigma}$ by comparing the products in the left-hand side of equation (35) for different harmonics, n. The value thus obtained is the exact membrane tension we are looking for. The bending elastic modulus, k_c, can be calculated thereafter from equation (35). The amplitudes of the fluctuations of *giant* vesicles are extremely sensitive to the presence of a very small membrane tension, as already mentioned by Schneider *et al.* [7]. For a vesicle of radius $R = 10^{-5}$ m (10 µm) and $k_c = 10^{-19}$ J a tension of $\sigma = 2 \times 10^{-5}$ mN/m leads to a two-fold decrease of the amplitudes of second harmonics, $U_2^m(t)$. For a small vesicle of radius $R = 10^{-8}$ m (100 Å) the tension producing the same effect is $\sigma = 20$ mN/m, a value one order of magnitude higher than the membrane rupture tension, $2 - 3$ mN/m, as reported by Kwok and Evans [2]. Due to the relation $\bar{p} \approx 2\bar{\sigma}$, the same two-fold decrease of $U_2^m(t)$ can alternatively be produced by osmotic effects of as low as 2×10^{-9} M concentration difference for a *giant* vesicle (10 µm), while 2 M are necessary for a *small* (100 Å) one. Therefore, the *small* vesicles are *always* fluctuating even under osmotic stresses that lead to membrane rupture !

3. Some experimental quantities.

Now we have to find a relation between the amplitudes, $\langle |U_n^m(t)|^2 \rangle$, and an experimentally measurable quantity. It is believed that what is seen under a phase contrast microscope is the cross-section of the vesicle membrane with the focal plane of the objective. Considering the equatorial cross-section of a vesicle with a plane through its center and parallel to the XY plane of our coordinate system, given by $\theta = \frac{\pi}{2}$ in equation (4), we can write :

$$\rho(\varphi, t) = R \left[1 + u \left(\frac{\pi}{2}, \varphi, t \right) \right] . \tag{36}$$

The mean radius of the equatorial cross-section, $\rho(t)$, at a given moment, t, is :

$$\rho(t) = \frac{1}{2\pi} \int_0^{2\pi} \rho(\varphi, t) \, \mathrm{d}\varphi \ . \tag{37}$$

Using the series (25, 21), after some algebra we obtain :

$$\rho(t) = R \left[1 + A_0^0 \, \Theta_0^0 \left(\frac{\pi}{2} \right) + \sum_{n=2}^{n_{max}} U_n^0(t) \, \Theta_n^0 \left(\frac{\pi}{2} \right) \right] \tag{38}$$

where :

$$\Theta_n^m(\theta) = (-1)^m \sqrt{\frac{2n+1}{4\pi} \frac{(n-m)!}{(n+m)!}} \, P_n^m(\cos\theta) \ .$$

Equation (38) shows that the equatorial cross-section radius fluctuates. This effect is mainly due to the vesicle deformations changing its shape from oblate to prolate and vice-versa. The time averaged radius, $\rho = \langle \rho(t) \rangle$, is easily calculated because the last term in (38) vanishes when averaged over the time. Using equation (29) (for a spherical vesicle $A_n^m = 0$ when $n \geqslant 1$), we finally have :

$$\rho = R \left[1 - \frac{1}{4\pi} \sum_{n=2}^{n_{max}} \sum_{m=-n}^{m=+n} \left\langle | U_n^m(t) |^2 \right\rangle \right] \ . \tag{39}$$

We see that the mean cross-section radius is equal to the mean vesicle radius, both being always smaller than the radius of a sphere of equivalent volume, an effect purely due to the existence of thermal fluctuations.

Following Bivas et al. [15] we calculate the normalized angular autocorrelation function of the vesicle radius, $\xi(\gamma, t)$, at a given moment of time :

$$\xi(\gamma, t) = \frac{1}{R^2} \left[\frac{1}{2\pi} \int_0^{2\pi} \rho(\varphi + \gamma, t) \rho^*(\varphi, t) \, \mathrm{d}\varphi - \rho^2(t) \right] \ . \tag{40}$$

Using the series expansions (25, 21), after some algebra we obtain the time averaged autocorrelation function :

$$\xi(\gamma) = \langle \xi(\gamma, t) \rangle = \sum_{n=2}^{n_{max}} \sum_{m \neq 0} \left\langle | U_n^m(t) |^2 \right\rangle Y_n^m \left(\frac{\pi}{2}, \gamma \right) Y_n^m \left(\frac{\pi}{2}, 0 \right) \ . \tag{41}$$

According to equations (24, 34), the amplitudes, $\left\langle | U_n^m(t) |^2 \right\rangle$, are not dependent on the index m. Taking advantage of this fact and using the addition theorem for the spherical harmonics [14], the sum on m can be explicitly performed and the above expression is transformed into the form :

$$\xi(\gamma) = \frac{kT}{4\pi k_c} \sum_{n=2}^{n_{max}} \frac{(2n+1)}{(n-1)(n+2)[\bar{\sigma} + n(n+1)]} P_n(\cos\gamma)$$

$$- \frac{kT}{k_c} P_0(\cos\gamma) \sum_{n=2}^{n_{max}} \frac{\left[\Theta_n^0 \left(\frac{\pi}{2} \right) \right]^2}{(n-1)(n+2)[\bar{\sigma} + n(n+1)]} \ . \tag{42}$$

This equation shows that the time averaged autocorrelation function, $\xi(\gamma)$, is a series of Legendre polynomials, $P_n(\cos\gamma)$, with coefficients given by the equipartition theorem,

equations (34). The term $(2n+1)$ reflects the fact that for each n there are $(2n+1)$ statistically independent m-modes. The last term in (42) compensates for the addition of all missing $m=0$ modes to equation (41) which are otherwise necessary for the addition theorem.

Up to now we were supposing that we knew the position of the vesicle center O, whose coordinates are given by equation (5). But observing (and measuring) only the equatorial cross-section it is not possible to calculate them because the complete $u(\theta, \varphi, t)$ is necessary. The best we can do is to calculate the coordinates, $(x'_0(t), y'_0(t))$, of the center O' of the observed equatorial contour.

Let (ρ, φ) and (ρ', φ') be the polar coordinates measured with respect to point O and O' respectively. By definition we have :

$$\frac{1}{2\pi} \int_0^{2\pi} \rho'(\varphi', t) \cos \varphi' \, d\varphi' = \frac{1}{2\pi} \int_0^{2\pi} \rho'(\varphi', t) \sin \varphi' \, d\varphi' = 0 . \qquad (43)$$

Let us denote the distance O'O by Rw, the angle it makes with the X axis by ψ, and the angle it is seen from a point on the contour by ϕ, (Fig. 1). The primed quantities can be expressed as functions of nonprimed ones and developed in series with respect to $w \ll 1$ and $\phi \ll 1$, keeping only the terms up to the second order. The quantities $w = w(t)$ and $\psi = \psi(t)$ are both unknowns that have to be determined from equations (43).

We calculate the radius, $\rho'(t)$, of the equatorial cross-section defined by equation (37), but now we use $(\rho'(\varphi', t), \varphi')$ instead of $(\rho(\varphi, t), \varphi)$:

$$\rho' = \langle \rho'(t) \rangle = R \left[1 - \frac{1}{4\pi} \sum_{n=2}^{n_{max}} \sum_{m=-n}^{m=+n} \langle |U_n^m(t)|^2 \rangle \right] +$$
$$+ R \left[\frac{1}{2} \sum_{n=2}^{n_{max}} \sum_{m=\pm 1} \langle |U_n^m(t)|^2 \rangle \left[\Theta_n^m \left(\frac{\pi}{2} \right) \right]^2 \right]. \qquad (44)$$
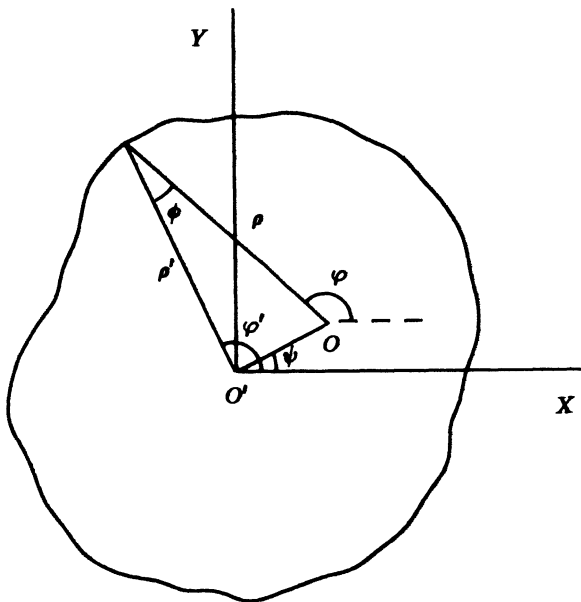

Fig. 1. — Cross-section of a vesicle in the plane (X, Y). O is the center of the vesicle, O' the center of the observed cross-section.

The first term in the above equation coincides with expression (39) and the last is a consequence of the fact that the center of the cross-section is fluctuating around the vesicle center. The displacement itself is a first order effect, given by $U_n^{\pm 1}(t)$ amplitudes, but its influence on the cross-section radius is of second order.

Using the same approach we calculate the experimental autocorrelation function, $\xi'(\gamma, t)$, given by the relation (40), but now we use $(\rho'(\varphi', t), \varphi')$ instead of $(\rho(\varphi, t), \varphi)$. Keeping only the terms up to the second order we calculate the experimental autocorrelation function, $\xi'(\gamma) = \langle \xi'(\gamma, t) \rangle$:

$$
\begin{aligned}
\xi'(\gamma) = {} & \frac{kT}{4 \pi k_c} \sum_{n=2}^{n_{\max}} \frac{(2n+1)}{(n-1)(n+2)[\bar{\sigma}+n(n+1)]} P_n(\cos \gamma) \\
& - \frac{kT}{k_c} P_1(\cos \gamma) \sum_{n=2}^{n_{\max}} \sum_{m=\pm 1} \frac{\left[\Theta_n^m\left(\frac{\pi}{2}\right)\right]^2}{(n-1)(n+2)[\bar{\sigma}+n(n+1)]} \\
& - \frac{kT}{k_c} P_0(\cos \gamma) \sum_{n=2}^{n_{\max}} \frac{\left[\Theta_n^0\left(\frac{\pi}{2}\right)\right]^2}{(n-1)(n+2)[\bar{\sigma}+n(n+1)]} .
\end{aligned}
\tag{45}
$$

We see that the experimentally calculated autocorrelation function has the same form as the theoretical one except the extra $P_1(\cos \gamma)$-term. Equation (45) shows that the angular autocorrelation function, $\xi'(\gamma)$, is a series of Legendre polynomials, $P_n(\cos \gamma)$, with theoretical coefficients $B_n(\bar{\sigma}, k_c)$:

$$
B_n(\bar{\sigma}, k_c) = \frac{kT}{4 \pi k_c} \frac{(2n+1)}{(n-1)(n+2)[\bar{\sigma}+n(n+1)]}, \qquad n \geqslant 2 .
\tag{46}
$$

Comparing with equation (24) we conclude that $B_n(\bar{\sigma}, k_c) = \frac{2n+1}{4\pi} \langle |U_n^m(t)|^2 \rangle$. Thus we have obtained the needed direct correspondence between the amplitudes of the vesicle fluctuations, $\langle |U_n^m(t)|^2 \rangle$, and the experimentally measured vesicle radius, $\rho'(\varphi', t)$, via the autocorrelation function, $\xi'(\gamma)$.

To find the value of the bending elastic modulus, k_c, we calculate the experimental autocorrelation function, $\xi'(\gamma, t)$, for each contour and, decomposing it into series of Legendre polynomials, we get the experimental coefficients, $B_n(t)$. We evaluate the mean values, $B_n = \langle B_n(t) \rangle$, and estimate the corresponding dispersions (standard deviations), D_n. Using $\bar{\sigma}$ and k_c as fitting parameters we minimize the function, $M(\bar{\sigma}, k_c)$:

$$
M(\bar{\sigma}, k_c) = \sum_{n=2}^{n=N+1} \left(\frac{B_n(\bar{\sigma}, k_c) - B_n}{D_n} \right)^2
\tag{47}
$$

where N is the number of amplitudes (harmonics) used for the fitting. As far as B_n values are an arithmetic mean of a very large number of experimental $B_n(t)$ data (usually 400 or more), their distribution is Gaussian, therefore, the quantity $M(\bar{\sigma}, k_c)$ obeys a χ^2 distribution with $(N-2)$ degrees of freedom. This fact can be used to verify the quality of the fit by comparing the calculated $M(\bar{\sigma}, k_c)$ value with the value of χ^2-distribution with $(N-2)$ degrees of freedom, taken from the statistical tables. It is practical to introduce the ratio of the two values, χ_R^2, and to compare it with unity. If $\chi_R^2 < 1$ the fit is acceptable otherwise it is rejected.

There is one more point that deserves a comment. The image formed by the microscope is projected onto the target of a video camera and is accumulated on it for the time between two successive scans, $t_s = 40$ ms. This integration leads to smearing of the fastly moving parts of the contour, and degradation of the resolution. If one suppose that the experimentally measurable radius, $\rho'(\varphi', t)$ is the mean value over the scan time :

$$\rho'(\varphi, t) = \frac{1}{t_s} \int_0^{t_s} \rho(\varphi, t + t') \, dt' \qquad (48)$$

the autocorrelation function, $\xi'(\gamma)$, averaged over the period of the observation, t_0, would be given by the expression :

$$\xi'(\gamma) = \frac{1}{2\pi t_0} \int_0^{t_0} \int_0^{2\pi} \left(\frac{1}{t_s} \int_0^{t_s} \rho(\varphi + \gamma, t + t') \, dt' \right) \times$$
$$\times \left(\frac{1}{t_s} \int_0^{t_s} \rho(\varphi, t + t'') \, dt'' \right) d\varphi \, dt \, . \quad (49)$$

This is in fact a triple integral with respect to the time in which we change the order of integration. Using the series expansions (25, 21) and making first the integration over the period of observation, t_0, one obtains an expression similar to (41), but now we have :

$$\langle U_n^m(t') U_n^{m*}(t'') \rangle = \langle |U_n^m(t)|^2 \rangle \frac{1}{t_s^2} \int_0^{t_s} \int_0^{t_s} \exp\left(-\frac{|t' - t''|}{\tau_n^m} \right) dt' \, dt'' \, . \qquad (50)$$

The integral in the last equation is the correcting factor due to the camera integration. If there was no such effect ($t_s = 0$) this factor would be 1 and we would obtain the previous result (41). The quantity τ_n^m is the correlation time of the respective modes calculated by Milner and Safran [10]. Comparing the expressions for the correlation time (see [10]) with that for the mean squared amplitudes (34) one can see that they are related :

$$\tau_n^m = \frac{4\pi\eta R^3}{kT} \left(2 - \frac{1}{n(n+1)} \right) B_n(\bar{\sigma}, k_c) \qquad (51)$$

where η is the viscosity of the medium surrounding the vesicle membrane. We see that, as a result of the camera integration, the value of the experimentally measured quantities, B_n', is modified by a factor depending on the ratio between the camera scan time, t_s, and the correlation time of the respective modes :

$$B_n' = 2 \left(\frac{\tau_n^m}{t_s} \right)^2 \left[\frac{t_s}{\tau_n^m} + \exp\left(-\frac{t_s}{\tau_n^m} \right) - 1 \right] B_n(\bar{\sigma}, k_c) \, . \qquad (52)$$

Using an iterative procedure, the best values of the correction factor and B_n were calculated from the experimental amplitudes B_n', and the corrected values, B_n were used in equation (47) to calculate the elastic modulus, k_c.

4. Sample preparation.

Egg-yolk phosphatidylcholine (EPC) was prepared according to the method of Singleton et al. [18], and dissolved in $CH_3OH/CHCl_3$ (1:9 v/v) at a concentration of 0.5 mg/ml. A small amount of this solution was sprayed on a microslide, then the solvent was removed under vacuum for about 1 hour. The microscope cell was prepared as already described in [15]

except a watertight material, about 0.1 mm thick, made up of the silicon product CAF4 (Rhône-Poulenc, France) was used as a spacer. Both the microslide and the cover slip were previously treated with trimethylchlorosilan (Sigma, U.S.A.) for making them hydrophobic. The cell was filled with deionized water (Millipore MQ, U.S.A.), and then sealed to avoid any evaporation. Giant vesicles were formed spontaneously in the cell, and generally they were studied one day to one week after the sample preparation.

5. Vesicle observation and image processing.

Giant vesicles were observed using an inverted phase contrast microscope IM35 (Carl Zeiss, F.R.G.) (objective PH 100 ×, NA = 1.25). The thermal fluctuations were monitored *via* a contrast-enhancing video camera C2400-07 (Hamamatsu Photonics, Japan) and recorded on a U-matic video tape recorder (Sony, Japan) for at least eight minutes. Video images, taken at regular time intervals of 1 s, were digitized with a Pericolor 2001 image processing system (Numelec, France). Digitized images were constituted of 512×512 8-bit pixels, and, with the magnification used, 1 pixel roughly corresponded to 0.1 μm. An out-of-focus image was usually subtracted from that of the vesicle to eliminate mottle or background heterogeneities. Digitized images were then transferred to a VAX-8600 computer (Digital, U.S.A.) for the determination of the contour coordinates. This was performed as in [8] by searching for the minimum intensity along the vesicle radius in given directions. In the conditions used, the contours appeared like a dark line of about 5 pixels width at half-height. In order to increase the accuracy on the contour determination, the vesicle radius in a given direction was calculated as the intensity-weighted average of the radii of these five points. The number of contour points so determined was roughly equal to the number of pixels constituting the contour, i.e. between 500 and 1000 depending on the vesicle size. An example of what can be obtained is shown in figure 2, where calculated contours have been superimposed to the digitized images of vesicles.
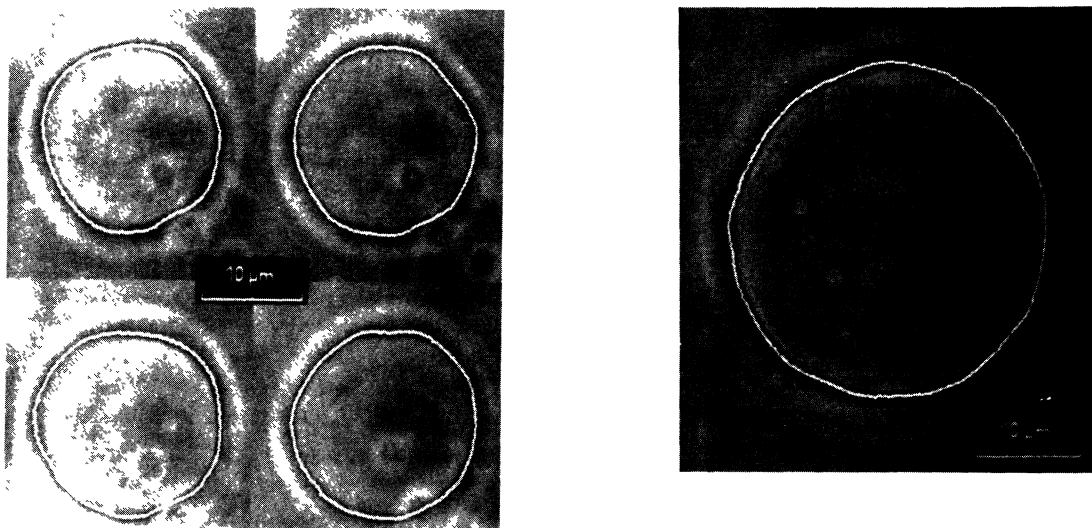

Fig. 2. — Images of two different vesicles obtained after digitization and background subtraction. The white line represents the calculated contour coordinates. Left figure : images taken at different time intervals of a vesicle having a mean radius of 8.45 μm, $k_c = 0.42 \times 10^{-19}$ J, $\bar{\sigma} = 22.6$. Right figure : picture of a vesicle having a mean radius of 14.05 μm, $k_c = 0.64 \times 10^{-19}$ J, $\bar{\sigma} = 93.3$.

The second step of the treatment was to eliminate the contours corresponding to noisy records, which can originate from a bad microscope focusing, for example. For this purpose, the experimental contours were roughly represented by a Fourier series limited to the first five terms. All the experimental points being farther than a chosen critical distance ($\simeq 2$ pixels) from that representation were deleted. If the number of deleted points for a given contour exceeded some value ($\simeq 5\%$), the whole contour itself was eliminated. Usually, less than 5 % of the total number of digitized images was lost after such manipulation. The rest were used for the determination of the bending elastic constant.

6. Numerical simulations.

The only way to check the validity of the theoretical model is to use the function (47) with as many different harmonics, B_n, as possible. It is obvious however, that due to the experimental limitations the number, N, of the harmonics that can actually be observed and investigated is limited. At least three important factors have to be considered : (i) the limited number of analysed images (contours), (ii) the precision on the contour coordinates, and (iii) the time resolution of video (40 ms) compared to the correlation times of the fluctuations modes. An easy way to estimate the effect of these different factors is to perform computer simulations.

In a first step, simulated contours were created without taking into account the third factor, i.e. video time. The theoretical values of the mean-squared Fourier amplitudes corresponding to a given set of values for k_c, $\bar{\sigma}$, and the mean vesicle radius were calculated as in [8]. The squared Fourier amplitudes for a given contour were obtained by multiplying these theoretical values by random numbers obeying a χ^2-distribution. These amplitudes were then randomly decomposed into the sine and cosine components of the Fourier series, which allowed the angular dependence of the radius of the simulated contour to be computed. A Gaussian noise could then be added to the vesicle radius, with a chosen standard deviation, in order to account for the experimental errors on the contour coordinates. These simulated contours were further analysed in the same way as the experimental ones.

An example of such a simulation is shown in figure 3. In this case, 40 contours, which roughly corresponds to the number used in the previous works [8, 15], have been generated
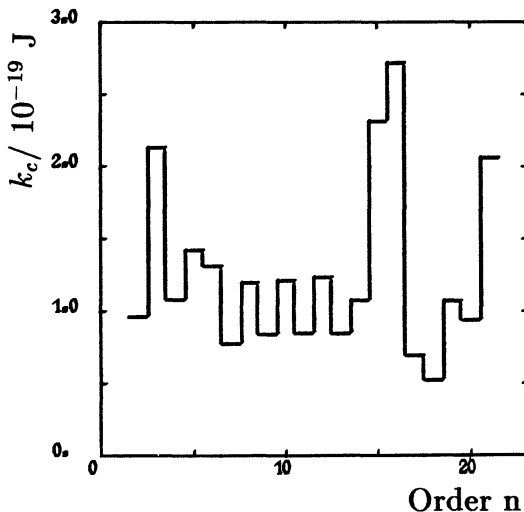

Fig. 3. — Simulated data : values of k_c *versus* the order n of fluctuations. 40 contours were generated, using $k_c = 10^{-19}$ J, $\bar{\sigma} = 0$, and a mean vesicle radius equal to 100 pixels. No noise was added to the calculated vesicle radii.

without any added noise. It is clear that the obtained values of k_c present large variations *versus n*, the order of the harmonics. However, when the number of generated contours is equal to 400, k_c remains rather constant up to $n \simeq 20$, as seen in figure 4, even in the presence of a Gaussian noise of 1 % on the vesicle radius. Such a noise corresponds to an error of 1 pixel on the radius for a 20 μm diameter vesicle, i.e. to the expected error in normal experimental conditions.
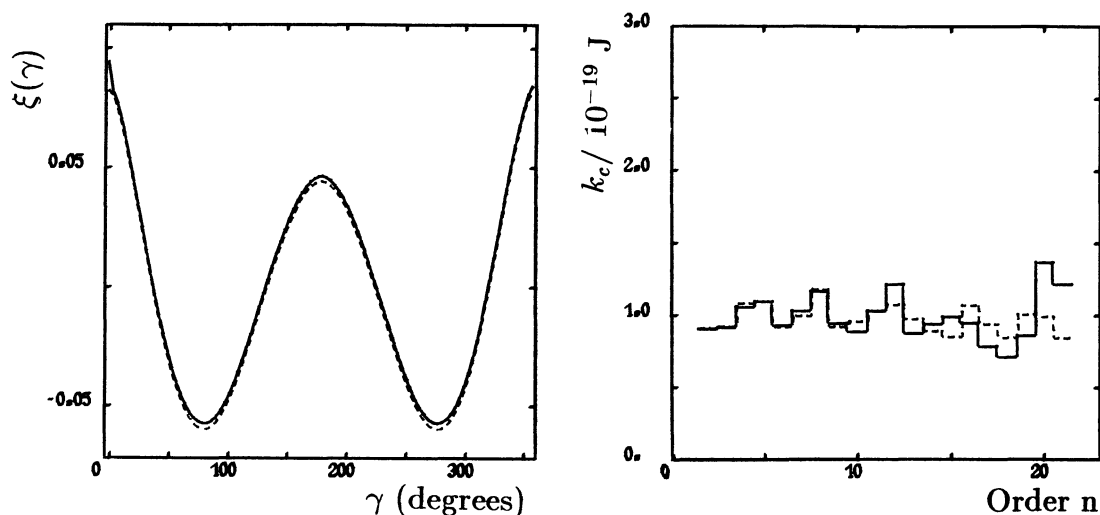

Fig. 4. — Simulated data : autocorrelation functions (left Fig.) and dependence of k_c *versus* the order *n* (right Fig.). Four hundred contours were generated, in the presence (*full line*) or absence (*dotted line*) of a Gaussian noise equal to 1 % on the vesicle radius. Entered values for simulations : $k_c = 10^{-19}$ J, $\bar{\sigma} = 0$, and mean vesicle radius = 100 pixels.

Another interesting point is worth mentioning. It can be seen that the autocorrelation functions obtained either with or without noise are almost identical, except in one point, $\gamma = 0$. So, the noise contributes to the autocorrelation function mainly in the form of a δ-function at $\gamma = 0$, as already pointed out in [15], and it has practically no effect on the values of k_c calculated from the Legendre amplitudes, B_n, of the autocorrelation function.

When the analysis of these simulated data is performed by direct Fourier decomposition of the contours, as in [8], the presence of noise leads to an important decrease of k_c for wavevectors $q \geqslant 8$ (Fig. 5). The noise contribution can be considerably reduced in this case as well, but an appropriate white noise have to be subtracted from the Fourier amplitudes, as shown in figure 5.

Finally, we should mention that the accurate value of k_c can be recovered from simulated contours generated with initial values of $\bar{\sigma}$ ranging from 0 to 200, even in the presence of a 1 % Gaussian noise on the vesicle radius (data not shown).

All the preceding simulations have been performed assuming that the time resolution of video is much higher than the frequency of the fluctuations, which is obviously not the case when high order harmonics are considered. So, an attempt has been done to quantify this effect by using the correction factor (52) derived above. As a first approximation, the theoretical mean-squared Fourier amplitudes of the contours were multiplied by this factor, taking the video time $t_s = 40$ ms, and using the relation (51) to calculate the correlation times
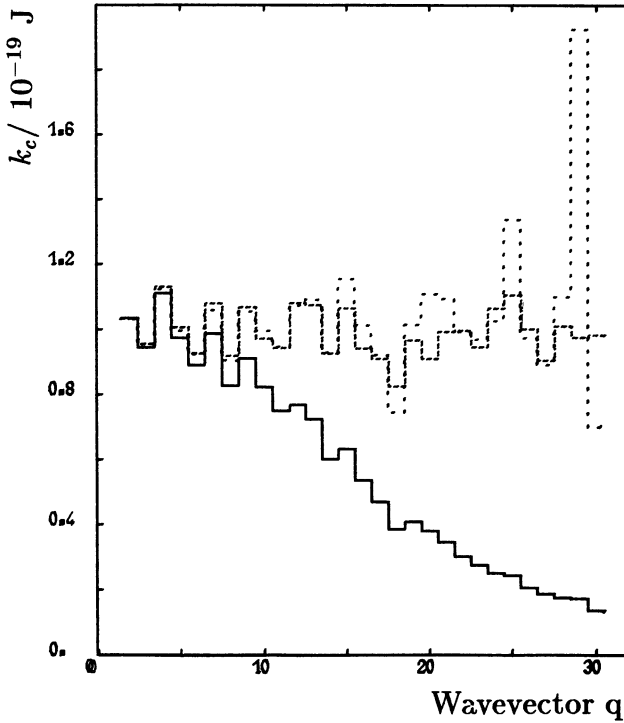
Fig. 5. — Analysis of simulated data by Fourier decomposition of the contours : (---------) without added noise on the vesicle radius ; (———) in the presence of a Gaussian noise of 1 % ; (- - - - - - -) in the presence of noise, after subtraction of an appropriate white noise from the Fourier amplitudes. Entered values for the simulations were the same as in figure 3.

τ_n^m of the respective modes. An example of what can be obtained is shown in figure 6, the entered values being in this case : $k_c = 0.5 \times 10^{-19}$ J, $\bar{\sigma} = 50$, vesicle radius $= 100$ pixels, Gaussian noise $= 1$ pixel. When the fit is done as usual, using only the $\chi_R^2 \leq 1$ criterion, 12 modes can be fitted (Fig. 6A, solid line), and this leads to $k_c = (0.71 \pm 0.05) \times 10^{-19}$ J and $\bar{\sigma} = 35 \pm 4$, i.e. to values clearly different from the entered ones. Moreover, a significant increase of k_c is observed when $n \geq 13$. On the contrary, if the fit is limited to the first few modes, whose correlation times are larger than the video time, the obtained values are nearly equal to the entered ones : for example, when $n = 2, ..., 7$, (correlation times ≥ 0.1 s), one obtains $k_c = (0.49 \pm 0.09) \times 10^{-19}$ J and $\bar{\sigma} = 57 \pm 15$ (Fig. 6A, dotted line). Finally, when the correction factor is introduced in the analysis of simulated data (Fig. 6A, dashed line), k_c remains constant up to $n = 20$, and the recovered value $k_c = (0.43 \pm 0.03) \times 10^{-19}$ J, is again very close to the entered one.

The results obtained by direct Fourier analysis of these simulated data are reported in figure 6B. The solid line represents the values of k_c versus the wavevector q of fluctuations, without taking into account the effect of $\bar{\sigma}$ and the white noise contribution. As expected, the entered positive value of $\bar{\sigma}$ leads to large values of k_c at low wavevectors. A plateau is observed for $q \simeq 10$ with $k_c \simeq 0.8 \times 10^{-19}$ J, then k_c decreases for $q \geq 19$. It is interesting to note that the decrease of k_c at high q is much less pronounced than in the case of figure 5, when the effect of integration time is not included. These data clearly demonstrate that the
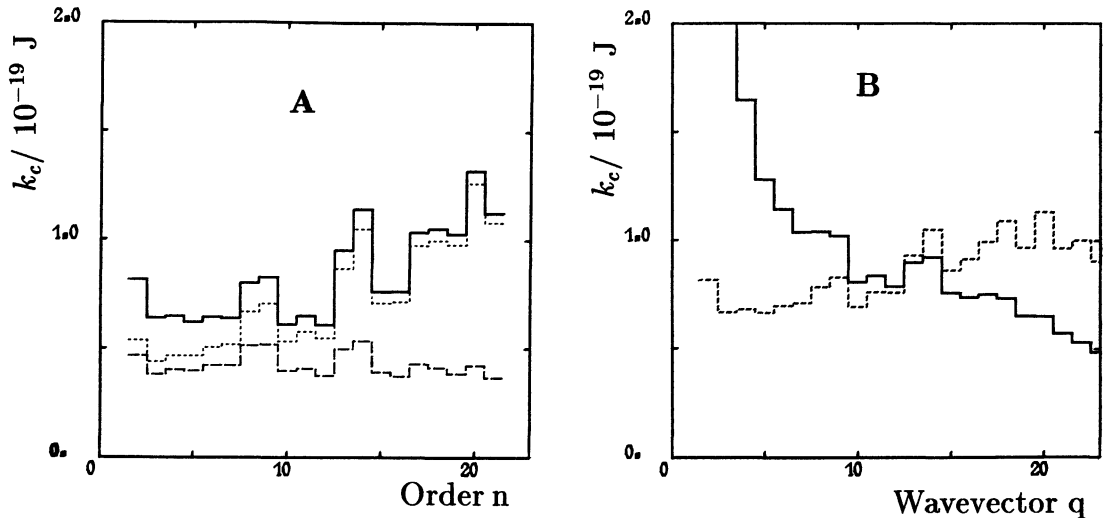
Fig. 6. — Simulated data : effect of the integration time of the video camera. (A) Values of k_c derived from the autocorrelation function : *full line* : using the $\chi_R^2 \leqslant 1$ criterion ; *dotted line* : considering only modes with $n \leqslant 5$; *dashed line* : after introducing the correction factor (Eq. (52)). (B) Values of k_c derived from the Fourier analysis of the contours : *full line* : rough analysis ; *dotted line* : after white noise subtraction and using $\bar{\sigma} = 35$.

contributions of the Gaussian noise and the effect of video integration time act in opposite way on the final result. However, in this case, the noise contribution prevails over the effect of correlation times, so that a decrease of k_c is still observed.

The dashed line in figure 6B represents the values of k_c obtained after white noise subtraction and after introducing $\bar{\sigma} = 35$. A constant value of $k_c \simeq 0.75 \times 10^{-19}$ J, once again very different from the entered one, is then obtained for $q \leqslant 12$.

7. Experimental results and discussion.

7.1 EXAMPLES OF GIANT EPC VESICLES. — An example of experimental data is shown in figure 7, for a vesicle of 19.4 µm in diameter : 384 contours have been analysed, either using the autocorrelation function and its decomposition into Legendre amplitudes B_n (Fig. 7A, B), or by direct Fourier analysis of the contours (Fig. 7C).

As can be seen in figure 7B, different behaviours are observed depending on the criteria used to fit the Legendre amplitudes, B_n, of the autocorrelation function. When the only criterium used is $\chi_R^2 \leqslant 1$, up to 16 amplitudes can be fitted (Fig. 7B, solid line), and $k_c = (0.69 \pm 0.03) \times 10^{-19}$ J with $\bar{\sigma} = 26 \pm 2$ is obtained. It is noteworthy that k_c increases for orders $n \geqslant 14$, as expected if the video time is larger than the correlation times of these modes. When the analysis is limited to the first few amplitudes, having correlation times larger than 0.16 s (i.e. at least fourfold larger than the video time), the dotted line in figure 7B, with $k_c = (0.44 \pm 0.1) \times 10^{-19}$ J and $\bar{\sigma} = 47 \pm 15$ is obtained. Finally, when the correction factor is used as described in the preceding section, a good fip up to $n = 21$ can be obtained, with $k_c = (0.40 \pm 0.02) \times 10^{-19}$ J and $\bar{\sigma} = 55 \pm 5$.

The Fourier analysis of the contours of the same vesicle is presented in figure 7C. When $\bar{\sigma}$ is taken equal to zero (solid line), k_c first decreases at low wavevectors, q, due to the small

excess area of the vesicle. Then a plateau is reached around $q \simeq 10$, and finally, an increase is observed for $q \geqslant 15$. In this case, therefore, the noise contribution to the measured Fourier amplitudes is smaller than the effect due to the video integration time. The comparison of the experimental data with the simulations for a vesicle of nearly the same characteristics, in the presence of 1 pixel Gaussian noise (Fig. 6B), seems to indicate that the experimental noise on the vesicle radius is significantly less than the indicated value.

Using $\bar{\sigma} = 26$, the dotted line in figure 7C is obtained, and $k_c = 0.7 \times 10^{-19}$ J remains practically constant for $q \leqslant 13$. The behaviour is quite similar to that obtained from the Legendre amplitudes of the autocorrelation function (Fig. 7B, solid line).
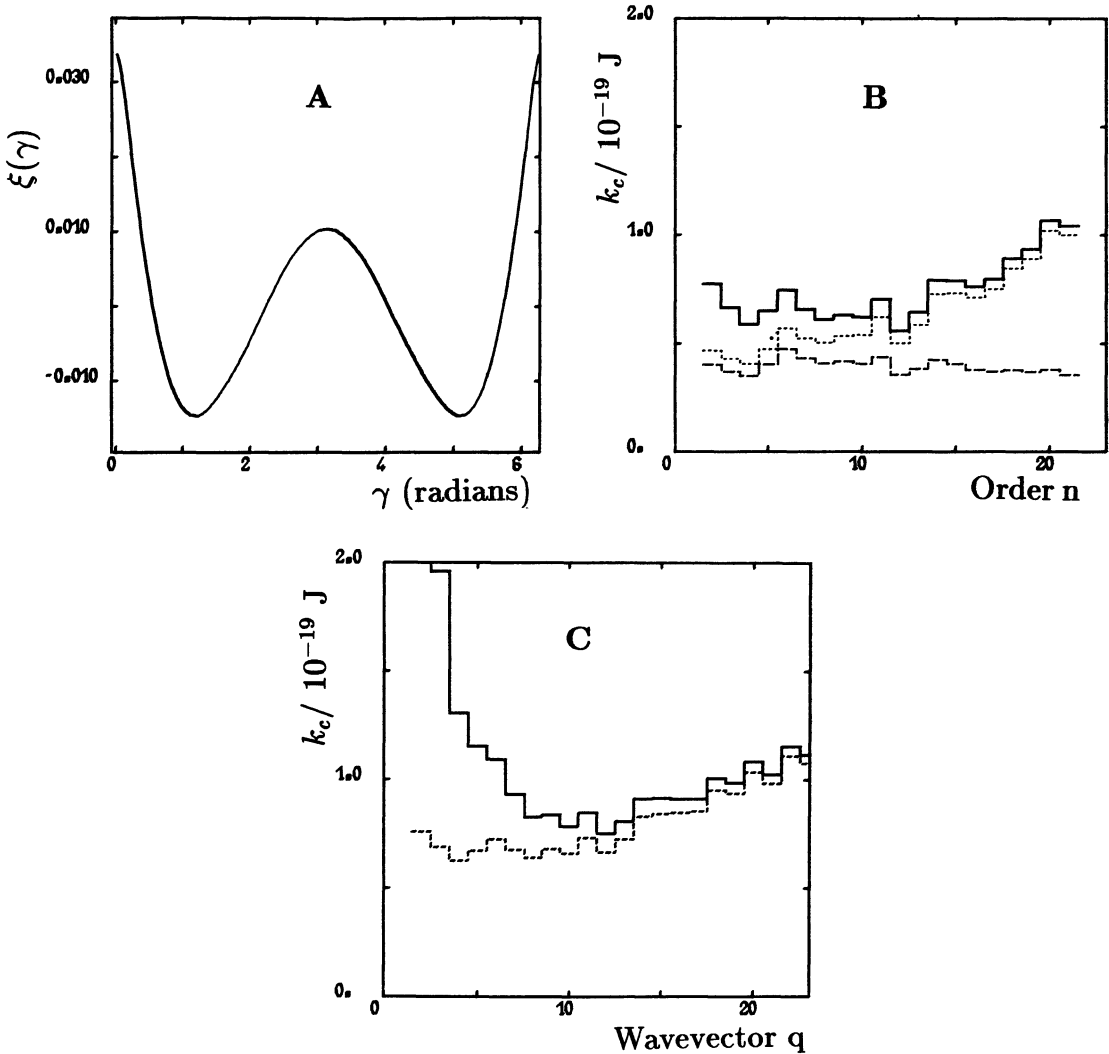

Fig. 7. — Example of experimental data obtained with a vesicle of 19.4 μm in diameter, and using 384 contours : (A) autocorrelation function $\xi(\gamma)$ of the fluctuations ; (B) dependence of k_c versus the order n, deduced from $\xi(\gamma)$: full line : using the $\chi_R^2 \leqslant 1$ criterion ; dotted line : considering only modes with correlation times larger than 0.16 s ; dashed line : after introducing the correction factor (Eq. (52)) ; (C) values of k_c derived from the Fourier analysis of the contours : full line : rough analysis ; dotted line : using $\bar{\sigma} = 26$.

7.2 EFFECT OF VIDEO INTEGRATION TIME : SUM OF DIGITIZED IMAGES. — It is clear from the above example that the video integration time constitutes a serious limitation in the study of fluctuating vesicles. Another mean to illustrate this effect is to increase at wish the characteristic time of video, which can be roughly done by adding successive digitized images before performing the analysis. Of course, it would be much better to act in the opposite way, i.e. to decrease the integration time. Unfortunately, this is not so easy.

The result from the analysis of contours obtained after such additions of digitized images is presented in figure 8. A vesicle of radius 14 μm was used in this case. The analysis has been performed either as usual, on single images (solid line), or after summing two (dotted line) or four (dashed line) successive images.

Figure 8A shows the dependence of k_c on n when the only criterion taken into account is $\chi_R^2 \leq 1$. In this case, the k_c value obtained increases from 1.0×10^{-19} J to 1.4×10^{-19} J and to 2.0×10^{-19} J for a single, sum of two and sum of four images, respectively.
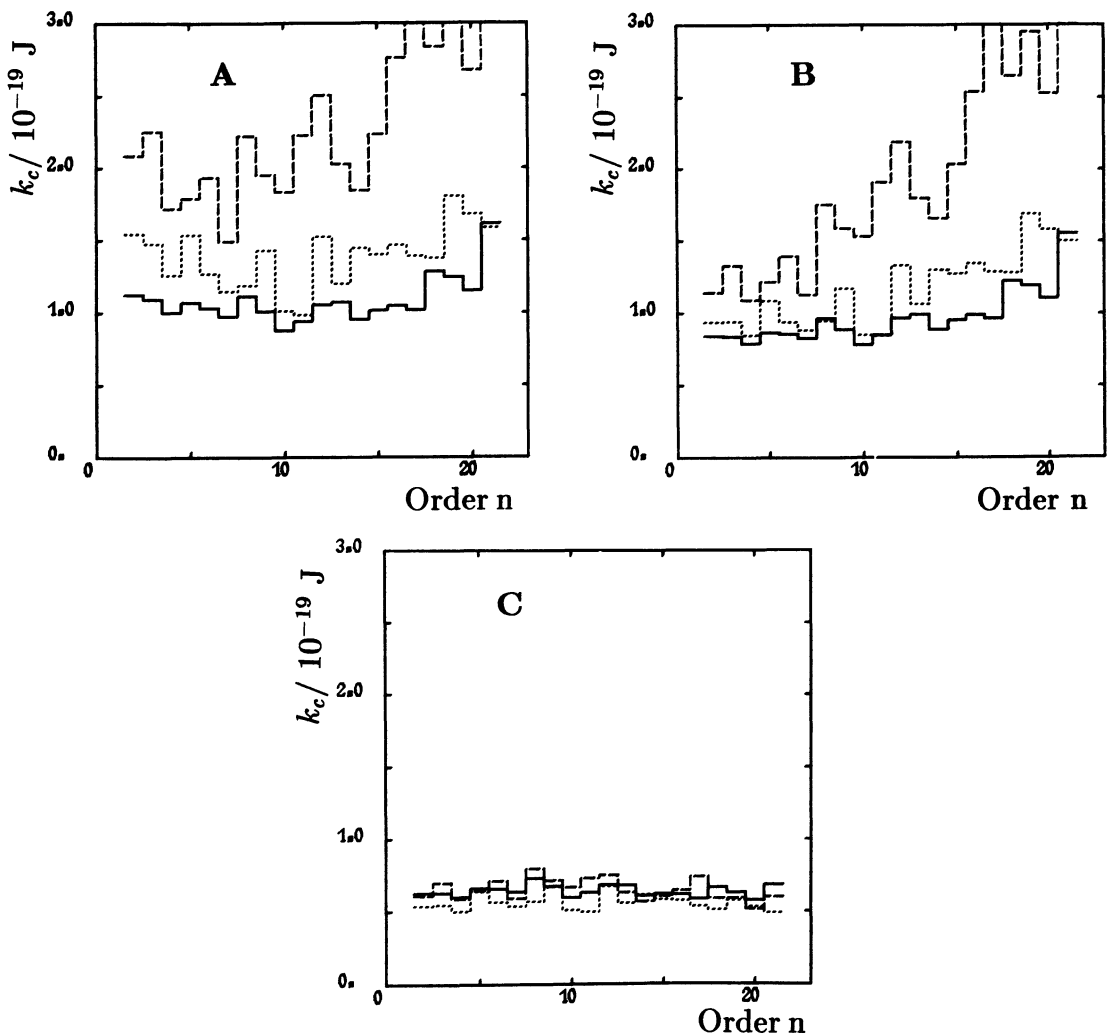

Fig. 8. — Values of k_c *versus* the order n of fluctuations obtained from the usual analysis (*full line*), or after summing 2 (*dotted line*) or 4 (*dashed line*) digitized images : (A) using the $\chi_R^2 \leq 1$ criterion ; (B) considering only modes with $n \leq 5$; (C) after introducing the correction factor (Eq. (52)).

When the analysis is limited to the first few amplitudes only (having the longest correlation times), figure 8B is obtained. The k_c values are very close to each other at low orders, therefore, the integration time has practically no effect on these modes. But, one can observe an increase of k_c with n, which is much larger when the number of added images is higher.

Finally, the correction factor has been introduced for the analysis of these data, using 40 ms, 80 ms, and 160 ms as integration times (depending on the number of summed images). As can be seen in figure 8C, the dependence of k_c on n is almost identical in the three cases considered here. Moreover, k_c remains practically constant up to $n \simeq 21$. This example is a strong support that the effect of the video integration time can be properly taken into account *via* the correction factor.

7.3 MEAN BEHAVIOUR OF GIANT EPC VESICLES. — An important characteristic of the analysis of thermal fluctuations, compared to the usual biophysical techniques, is that it does not deal with large populations of vesicles, but on the contrary with individuals. So, it is quite necessary to check both the reproducibility of the method and an eventual variability of the system, by studying the behaviour of a number of vesicles. For this purpose, thermal fluctuations of 62 giant EPC vesicles have been recorded and analysed. Among all these vesicles, 14 led to negative values of $\bar{\sigma}$ and could not be well fitted. The 48 remaining vesicles have been analysed using different criteria, as described below. The obtained results are presented in the form of normalized distributions of the obtained k_c values. These histograms have been constructed by summing the individual contributions of each vesicle, which have been assumed to be Gaussian distributions centered on the respective k_c values deduced from Legendre amplitudes B_n, with standard deviations equal to errors estimated from the goodness of the fit.

Disregarding any effect related to experimental limitations, the « best » vesicles should be those leading to a good fit ($\chi^2_R \leqslant 1$) on the maximum number of amplitudes ($N \geqslant 20$). Seventeen vesicles fulfil these conditions and lead to the histogram plotted in figure 9A. As can be seen, the histogram is constituted of two ill-defined peaks, the first one centered at $(0.69 \pm 0.06) \times 10^{-19}$ J, and the second one, much more important, at $(1.02 \pm 0.13) \times 10^{-19}$ J.

On the contrary, if one takes into account the problem of video integration time, the best values of k_c must be obtained by limiting the analysis to the modes having correlation times much longer than 40 ms. This has been done by considering only those harmonics whose correlation time was larger than 160 ms, and selecting only the vesicles satisfying this condition up to at least $n = 5$. In this case, one obtains the histogram of figure 9B, with only 10 vesicles. The main peak of this histogram corresponds to $k_c = (0.53 \pm 0.11) \times 10^{-19}$ J. Two other minor peaks can also be distinguished, at $(0.91 \pm 0.17) \times 10^{-19}$ J and $(1.45 \pm 0.15) \times 10^{-19}$ J. It is interesting to notice that these values are about twofold and threefold larger than that of the first peak. It must be mentioned that increasing the threshold time to 300 ms leads to a smaller value $k_c = 0.45 \times 10^{-19}$ J. However, only five vesicles can then be fitted.

Finally, the vesicles have been analysed using the correction factor as already discussed. However, only the amplitudes corrected by less than a twofold factor have been considered. In these conditions, as many as 42 vesicles can be correctly fitted on more than 5 amplitudes with $\chi^2_R \leqslant 1$, and the obtained distribution of k_c is plotted in figure 10A. The best fit of this histogram using a sum of three Gaussian distributions (dotted line) leads to $k_c = (0.4 \pm 0.04) \times 10^{-19}$ J, $(0.51 \pm 0.16) \times 10^{-19}$ J, and $(1.3 \pm 0.2) \times 10^{-19}$ J. Thus, the two first populations are not clearly distinguished, and can be fitted by a single Gaussian with $k_c = (0.43 \pm 0.11) \times 10^{-19}$ J. It is worth mentioning that almost the same value for
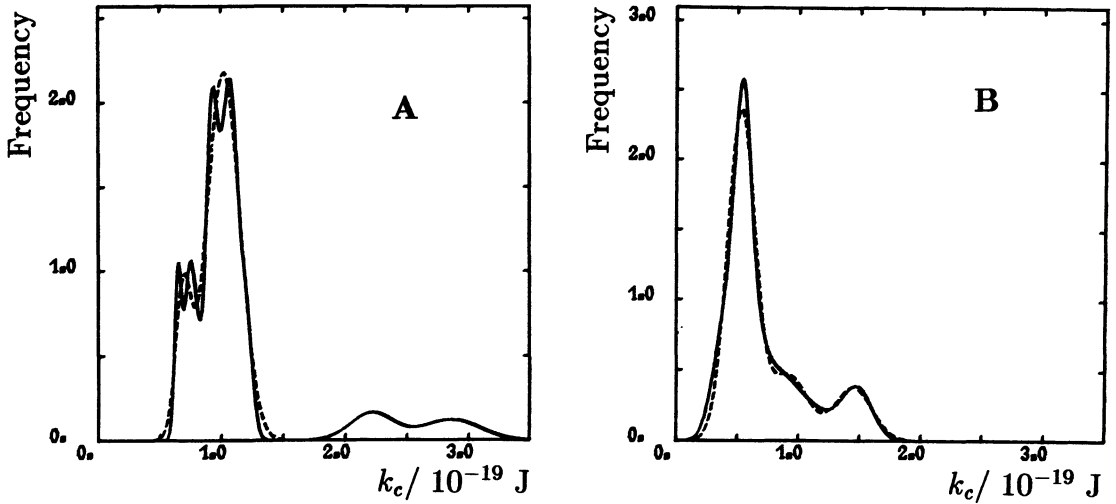
Fig. 9. — Histograms of k_c values, obtained : (A) with 17 vesicles fitted up to $n = 21$ with $\chi_R^2 \leq 1$; (B) with 10 vesicles fitted up to at least $n = 5$, with the correlation times of these modes ≥ 0.16 s. The *full lines* represent the experimental histogram, and the *dotted lines* correspond to the best fits obtained using a sum of 2 (A) or 3 (B) Gaussian distributions (see text).
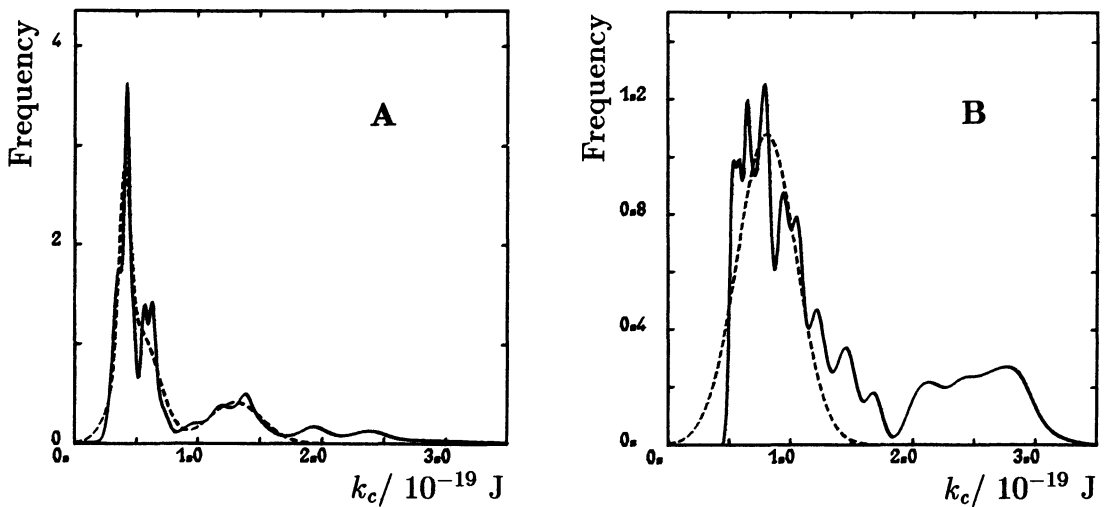

Fig. 10. — Histograms of k_c values, obtained : (A) with 42 vesicles fitted up to at least $n = 6$, using the correction factor for the integration time of the camera (Eq. (52)), with $\chi_R^2 \leq 1$; (B) with the same 42 vesicles fitted up to at least $n = 5$ with $\chi_R^2 \leq 1$, but without using the correction factor. The *full lines* represent the experimental histogram, and the *dotted lines* correspond to the best fits obtained using a sum of 3 (A) or 1 (B) Gaussian distributions (see text).

k_c is obtained by considering only the long correlation time amplitudes. For comparison, the histogram obtained with the same vesicles, but without correction factor and using as criterion only $\chi_R^2 \leq 1$ on at least 4 amplitudes, is represented in figure 10B. As can be seen, the

distribution is then very broad and, when fitted with a single Gaussian, the first peak leads to $k_c = (0.80 \pm 0.24) \times 10^{-19}$ J.

It is interesting to consider the behaviour of some other physical properties of the studied vesicles. The size distribution of the 42 vesicles well-fitted using the correction factor is represented in figure 11A. Their diameters range from about 10 μm to 40 μm, with a maximum centered around 20 μm. However, when the criterion used is the correlation time of harmonics, as in the histogram of figure 9B, only the large-size vesicles (with diameters larger than 18 μm, dotted line in Fig. 11A), are retained.

The membrane tension can be calculated from $\bar{\sigma}$, using equation (15). As shown in figure 11B, the distribution is broad with values between $(0 - 15)10 \times ^{-5}$ mN/m for most of the analysed vesicles. An interesting point is that the long correlation time vesicles exhibit a sharper distribution, at low values of the membrane tension $(0 - 3) \times 10^{-5}$ mN/m.
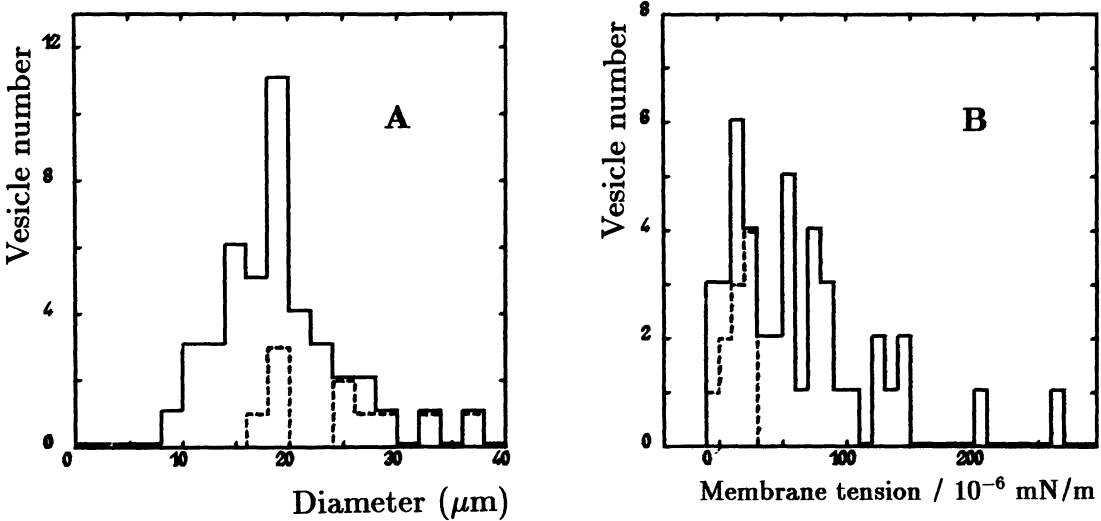

Fig. 11. — Size (A) and membrane tension (B) distributions of the studied vesicles. The *full line* corresponds to the 42 vesicles represented in the figure 9A, and the *dotted line* to the 10 vesicles of figure 8B.

8. Conclusion.

The main conclusion that can be drawn from the above results is that thermal fluctuations of giant vesicles constitute a useful tool to quantify the bending elasticity of lipid bilayers, provided that some requirements are fulfilled, both at experimental and theoretical levels.

First, fluctuation amplitudes being random variables, the precision is directly related to the number of analysed contours. As illustrated by simulations, several hundred contours must be digitized and analysed to obtain a good accuracy. With the experimental set-up used in our laboratory, this can be routinely done in about 1-2 hours, which is not too much time-consuming. Future development, based on real-time image processing, should still considerably increase these technical capabilities.

Another important point is the precision on the contour coordinates, which depends on the magnification used and on the resolution of the microscope, the camera, the video tape recorder, and the image digitizer. However, simulations clearly show that, as far as the error

on the vesicle radius is a random Gaussian noise, its contribution is almost completely cancelled by the use of the autocorrelation function and of its decomposition into associated Legendre amplitudes, which remain statistically significant on more than 20 modes. On the contrary, the noise largely contributes to the mean-squared Fourier amplitudes of the contours, resulting in an apparent decrease of the calculated k_c values for wavevectors $q \geqslant 8$. This effect can be readily corrected, at least in *simulated* data, by subtracting an appropriate level of white noise from the Fourier amplitudes. However, in the case of *experimental* data, this becomes much more difficult, if not impossible, due to the occurence of another experimental limitation, the camera integration time, which acts in the opposite way.

Indeed, as already stressed in [9], the camera integration time, $t_s = 40$ ms, is expected to decrease the amplitudes of modes having correlation times of the same order of magnitude as, or smaller than t_s. Both simulated and experimental data clearly show that this effect cannot be ignored in the analysis of thermal fluctuations. Two attempts can be made to overcome this difficulty. The first one consists of limiting the analysis to the harmonics having $\tau_n^m \gg t_s$. However, this method, which *a priori* looks quite satisfactory, suffers from some serious disadvantages. Indeed, if one considers a vesicle of 10 μm in diameter, which corresponds to the typical size in previous studies, one can calculate that τ_n^m decreases from 0.95 s for $n = 2$ down to about 40 ms for $n = 6$, in the favorable case : $\bar{\sigma} = 0$ and $k_c = 0.5 \times 10^{-19}$ J. Fortunately, τ_n^m is proportional to the third power of the vesicle radius, so this kind of analysis can be nevertheless performed, provided that large enough vesicles of low membrane tension are available. This limitation is well-illustrated in figure 11, which shows that only vesicles of about 20 μm or more, with $\sigma \leqslant 3 \times 10^{-5}$ mN/m, satisfy such drastic conditions. Moreover, even with these very large vesicles, only few amplitudes can be analysed, typically between 4 and 7. This necessarily leads to a loss of precision in determining k_c and $\bar{\sigma}$, and to a broadening of the final histogram.

Another way of taking into account the effect of the integration time is to introduce a correction factor in the analysis, as described in section 3. The validity of this factor is entirely based on the assumption that the experimentally determined contours correspond to the mean values of the actual contours over the integration time, a hypothesis not quite obvious. However, at least two features argue for the usefulness of this correction : (i) it leads to values of k_c very close to those obtained from the long correlation time harmonics, and (ii) it allows the « good » value of k_c to be recovered after summation of two or four digitized images, provided that the integration time t_s is multiplied by a factor two or four, respectively.

At the theoretical level, it is now clear that the assumption for the independence of the different fluctuation harmonics, made in previous studies [9, 15], is not tenable in view of the experimental data. Indeed, large variations in the k_c values are obtained at low orders, even when the experimental limitations described above can be neglected. A complete and exact theory has been developed here to account for both constraints that are exerted upon thermal fluctuations, namely the constant area and constant volume of the vesicle. This has been done *via* two Lagrange multipliers related to the membrane tension and hydrostatic pressure difference. However, these two parameters are not independent, and only one of them, either $\bar{\sigma}$ or $\bar{p}$, has to be considered. Hence, the final expression for k_c is almost the same as that proposed in [10]. This theoretical model holds for all the vesicles having positive values of $\bar{\sigma}$, i.e. for a spherical average contour.

Finally, applying this method to a relatively large number of giant EPC vesicles, one obtains for the bending modulus a value : $k_c = (0.40 - 0.53) \times 10^{-19}$ J, with membrane tensions ranging below 15×10^{-5} mN/m. First, it is noteworthy that these membrane tensions are extremely low, experimentally undetectable by classical techniques. Nevertheless, they

modify considerably the amplitudes of thermal fluctuations, and must absolutely be taken into account. This is illustrated in figure 2, where the contours of two vesicles having different values of $\bar{\sigma}$ are reported : deformations are clearly larger in the case of $\bar{\sigma} = 22.6$ (top figure) compared to $\bar{\sigma} = 93.3$ (bottom figure). On the other hand, the value obtained for k_c is of the same order as those previously reported [9, 15]. However, it must be stressed that all the above-mentioned problems, both at the experimental and theoretical levels, have been for the first time taken into account in the analysis, which strongly supports the reliability of the obtained results. Indeed, it is clear that, in the case of the direct Fourier transform of the contours, as performed in [9], the noise contribution together with the effects of $\bar{\sigma}$ and of the video integration time can balance each other, and lead to an apparent constancy of k_c in some range of wavevectors q. The obtained value of k_c, therefore, reflects these three contributions, in addition to the true bending elasticity. The autocorrelation function of the fluctuations has already been used in [15]. However, a global fit of this function, instead of its decomposition into Legendre amplitudes, was done without considering the effect of nonzero membrane tension, $\bar{\sigma}$. Thus, the derived value of k_c was mainly dependent on the behaviour of the 2nd harmonic, which is extremely sensitive to the variations of the membrane tension.

In conclusion, it can be stressed that most of the conditions required to truly extract the bending elasticity of lipid bilayers from thermal fluctuations can be fulfilled : analysis of a large number of contours to obtain a meaningful statistics, suppression of the noise contribution, use of an appropriate mathematical model to take the effect of membrane tension into account. The only remaining limiting factor in the proposed method is the integration time of standard video devices. As shown above, this difficulty can be overcome either by considering only the first harmonics of very large vesicles having low membrane tensions, or by using a proper correction factor. However, it would be much more satisfactory to decrease the integration time of the experimental set-up, down to about 1 ms. This last major improvement is currently under investigation in our laboratory.

References

[1] HELFRICH W., *Z. Naturforsch.* **28c** (1973) 693.
[2] KWOK R. and EVANS E., *Biophys. J.* **35** (1981) 637.
[3] EVANS E. and NEEDHAM D., *Faraday Discuss. Chem. Soc.* **81** (1986) 267.
[4] SERVUSS R. M., HARBICH W. and HELFRICH W., *Biochim. Biophys. Acta* **436** (1976) 900.
[5] SAKURAI I. and KAWAMURA Y., *Biochim. Biophys. Acta* **735** (1983) 189.

[6] SCHNEIDER M. B., JENKINS J. T. and WEBB W. W., *Biophys. J.* **45** (1984) 891.
[7] SCHNEIDER M. B., JENKINS J. T. and WEBB W. W., *J. Phys. France* **45** (1984) 1457.
[8] ENGELHARDT H., DUWE H. P. and SACKMANN E., *J. Phys. Lett. France* **46** (1985) L-395.
[9] DUWE H. P., ENGELHARDT H., ZILKER A. and SACKMANN E., *Mol. Cryst. Liq. Cryst.* **152** (1987) 1.
[10] MILNER S. T. and SAFRAN S. A., *Phys. Rev. A* **36** (1987) 4371.
[11] DEULING H. J. and HELFRICH W., *Biophys. J.* **16** (1976) 861.
[12] DEULING H. J. and HELFRICH W., *J. Phys. France* **37** (1976) 1335.
[13] HARBICH W., DEULING H. J. and HELFRICH W., *J. Phys. France* **38** (1977) 727.
[14] ARFKEN G., Mathematical Methods for Physicists (Academic Press, New York - San Francisco - London) 1970.
[15] BIVAS I., HANUSSE P., BOTHOREL P., LALANNE J. and AGUERRE-CHARIOL O., *J. Phys. France* **48** (1987) 855.
[16] HELFRICH W., SERVUSS R. M., *Nuovo Cimento* **3D** (1984) 137.
[17] JENKINS J. T., *J. Math. Biol.* **4** (1977) 143.
[18] SINGLETON W. S., GRAY M. S., BLOWN M. L. and WHITE J. L., *J. Am. Oil Chem.* **42** (1965) 53.
[19] FAUCON J. F., MÉLÉARD P., MITOV M. D., BIVAS I., BOTHOREL P., *Colloid and Polym. Sci.* (in press).